FIBER-MATRIX INTERFACE DEBONDING CHARACTERIZATION USING A DUAL-VISION SYSTEM

H Girard, Milena Tosti Umemura, Aurélien Doitrand, Nathalie Godin, R G Rinaldi, Behrad Koohbor, Jérôme Bikard

FIBER-MATRIX INTERFACE DEBONDING CHARACTERIZATION USING A DUAL-VISION SYSTEM

H. Girard[1], M. Tosti-Umemura[1], A. Doitrand[1], N. Godin[1], R.G. Rinaldi[1], B. Koohbor[2] and J. Bikard[3]

[1]INSA-Lyon, Universite Claude Bernard Lyon 1, CNRS, MATEIS,
UMR5510, 69621, Villeurbanne, France
Email: hugo.girard@insa-lyon.fr, milena.umemura@insa-lyon.fr aurelien.doitrand@insa-lyon.fr
nathalie.godin@insa-lyon.fr and renaud.rinaldi@insa-lyon.fr
[2]Axel'one (Solvay),
87 Avenue des Frères Perret, CS 70061, 69192 Saint Fons, France
Email: jerome.bikard@solvay.com
[3]Department of Mechanical Engineering,
Rowan University, 201 Mullica Hill Rd., Glassboro, NJ 08028, United States of America
Email: koohbor@rowan.edu

Keywords: Fiber-matrix, interface, debonding, characterization

Abstract
Fiber-matrix interface debonding is characterized experimentally using single transverse glass fiber within an epoxy matrix specimen tested under uniaxial tension. A dual-vision system, consisting of two synchronized cameras, is used to monitor the initiation and propagation of the fiber-matrix debonding as a function of the applied remote loading. Debonding was found to initiate at the free surface to tunnel at the fiber pole. Debonding topologies are characterized in terms of maximum opening and through thickness length and angle. The debonding angles are challenging to determine experimentally, so that a numerical model is established, which validated the accuracy of the experimental measurements.

1. Introduction

Fiber-matrix interface in composite materials is known to play a major role in the damage and associated ultimate properties. Indeed, stress concentration resulting from elastic mismatch, proximity to adjacent fibers, and low fracture properties can rapidly induce damage at the interface. Therefore, it is crucial to accurately characterize their fracture properties.

Fiber-matrix interface fracture characterization can be achieved using single-fiber tests such as, *e.g.*, multi-fragmentation or pull-out tests [1]. Fiber-matrix interface primarily undergoes shear loading using above-mentioned methods. However, tensile properties are as important and require other characterization methods to be used. Single-fiber sample loaded transversely can be used to assess opening fracture properties. Koyanagi *et al*. [2] used the debonding length and cohesive zone model to identified fracture properties. Authors reported the difficulty in identifying the debonding shape due to compression loading on the fiber equators. Debonding monitoring may thus require more in-depth characterization method to enable accurate inverse identification.

Livingston and Koohbor [3] performed experimental observations of macro-scale debonding. Single-fiber composite specimens were tested under uniaxial tension and full-field measurements at the fiber vicinity was performed to observe debonding stages. For this purpose, DIC was used to extract local strain fields and debonding angle at the free surfaces as a function of the applied loading [4]. However, debonding observations are limited to the front surface which provides limited information on the complete debonding process.

The present work thus improves the above-discussed experimental investigation of fiber-matrix interface by using a dual-vision approach to enable the simultaneous characterization of in-plane and through-thickness debonding process in single macro fiber model composites. Section 2 details the experimental set-up along with samples preparation. Results obtained from the debonding characterization are presented and confronted to numerical simulations to be further discussed in Section 3. Finally, conclusions on the proposed approach are drawn.

2. Experiments

2.1. Materials and sample preparation

Single fiber samples are made by embedding a 1 mm diameter quartz glass fiber in a translucid, room-curable epoxy. The epoxy resin (SD2505/SR1500, Sicomin, France) is cured at room temperature for one month to ensure that the resin is fully cured. Isotropic elastic properties of the fiber and the matrix are given in Table 1. Elastic properties of the epoxy matrix are determined in-house, using 5 tensile fiber-free samples prepared under the same curing conditions. The final sample, whose geometry is shown in Figure 1, has a 5 mm wide and 5 mm thick cross-section.

Table 1. Elastic properties of the matrix and fiber.

Property	Epoxy	Glass fiber
Young's modulus [GPa]	2.7 ± 0.2	72
Poisson's ratio	0.41 ± 0.04	0.3

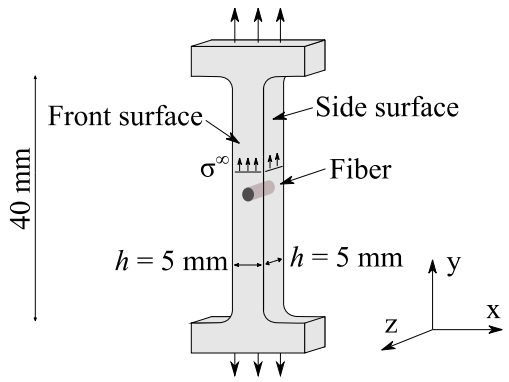

Figure 1. Single fiber specimen geometry and dimensions.

The single fiber is held in place using a 3D-printed jig. The surface of the fiber is cleaned with isopropanol to remove any unwanted substances from the surface. The matrix is poured into a silicone mold, where the latter is drilled at the location of the fiber to allow it to protrude from the final sample. This eliminates the need to polish the end of the fiber itself. The front surface of the sample is slightly polished with fine sandpaper with a grain size of approximately 8 µm. The side surfaces are also polished, first using similar fine sandpaper, then using a rotating cotton disc coupled with a polishing solution to obtain a perfectly transparent, flat side surface. The front surface is then spray painted for DIC. Samples are tested under tension at room temperature at a constant displacement rate of 0.18 mm/min. A dual-vision system consisting of two perpendicularly positioned cameras (FLIR Grasshopper GS3-U3-41C6M-C) is installed. This allows simultaneous observation of the front and side surfaces of the sample.

2.2 Mechanical test and image-based measurements

Figure 2 shows the parameters describing debonding geometry. Since straight-faced samples are used, debonding is likely to initiate at the free surface [5]. Debonding can be described by the debonding angle θ_{d} at the free face, measured by the angle between the two debonding tips. The quantity δ_{nn} corresponds to the maximum normal debonding opening. It is worth noting that considering the samples geometry and loading condition, maximum opening will occur at the pole of the fiber. The debonding opening actually reflects the distance separating the two lips of the crack. The length of debonding through the thickness is described by l_{d}, which corresponds to the length of debonding in the z-direction at the pole of the fiber.

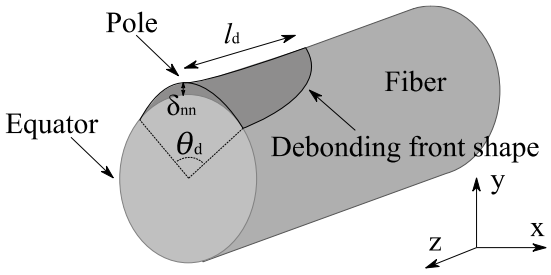

Figure 2. Fiber-matrix debonding geometrical parameters.

The debonding length determination consists in observing and monitoring the debonding propagation through the thickness of the sample, *i.e.*, in the z-direction. Since the debonding is likely to initiate and propagate at the fiber pole with respect to the loading direction due to the maximum stress attained at this location, the latter also corresponds to the maximum possible debonding length l_{d}. The method used to determine the debonding length makes use of the image processing free software, ImageJ. The side images are first imported into the software, then aligned to eliminate any motion induced by the tensile test, with the images shifted to match the previous one. In this way, the location of the fibers remains constant for several remote stresses, which facilitates identification of the debonding. The image preceding the onset of debonding is then selected, from which the gray level difference for each pixel is calculated with the subsequent images. As a result, the debonding area results in a large gray level difference compared to the initial image, while the other areas result in a difference close to 0. A threshold of 17% in gray level intensity is then applied to the difference between the two images and superimposed on the real image. The threshold value is set so that the results coincide with the visual observation of a large debonding surface. The new images highlight the debonded area, which length is determined as the maximum distance within the threshold area.

Maximum debonding opening is determined using the displacement fields deduced from DIC measurement. In details, a camera is positioned parallel to the sample front surface. The approach involves the use of Ufreckles software [6], from which displacement fields can be derived. A virtual gauge aligned with the loading direction and passing through the fiber and the matrix at the top pole is positioned. The U_{y} displacement is determined along the gauge as a function of the applied remote load within both the fiber and matrix. From a certain loading level, displacement discontinuously develops at the fiber-matrix interface, which can be associated with debonding initiation. From this loading level, the displacement remains almost constant within either the matrix or the fiber, allowing the debonding opening δ_{nn} to be assessed by computing the displacement jump.

The debonding angle remains difficult to observe because it is characterized by sub-pixel mechanisms that cannot be captured either by optical observation or by the DIC residuals. As a consequence, inverse calculation based on elastic calculations performed on a 3D numerical is used to determine the debonding angle.

3. Results and discussion

The following results are presented for one sample to illustrate the characterization approach. Since debonding is likely to initiate from the free surfaces of the sample at the pole of the fiber relative to the loading direction, 4 preferred initiation sites can be defined. For the sake of simplicity, only the first debonding site is considered in what follows.

Figure 3a shows multiple side images illustrating the debonding process, with both raw and thresholded images, left and right images, respectively, for different loading level σ^{∞}. The location of the crack tip is highlighted by a red triangle marker, enabling the debonding length to be determined as the distance

to the free surface. Notably, the fiber from the studied sample is slightly tilted, approximately 4 deg. relative to the loading direction, potentially influencing the debonding shape topology.

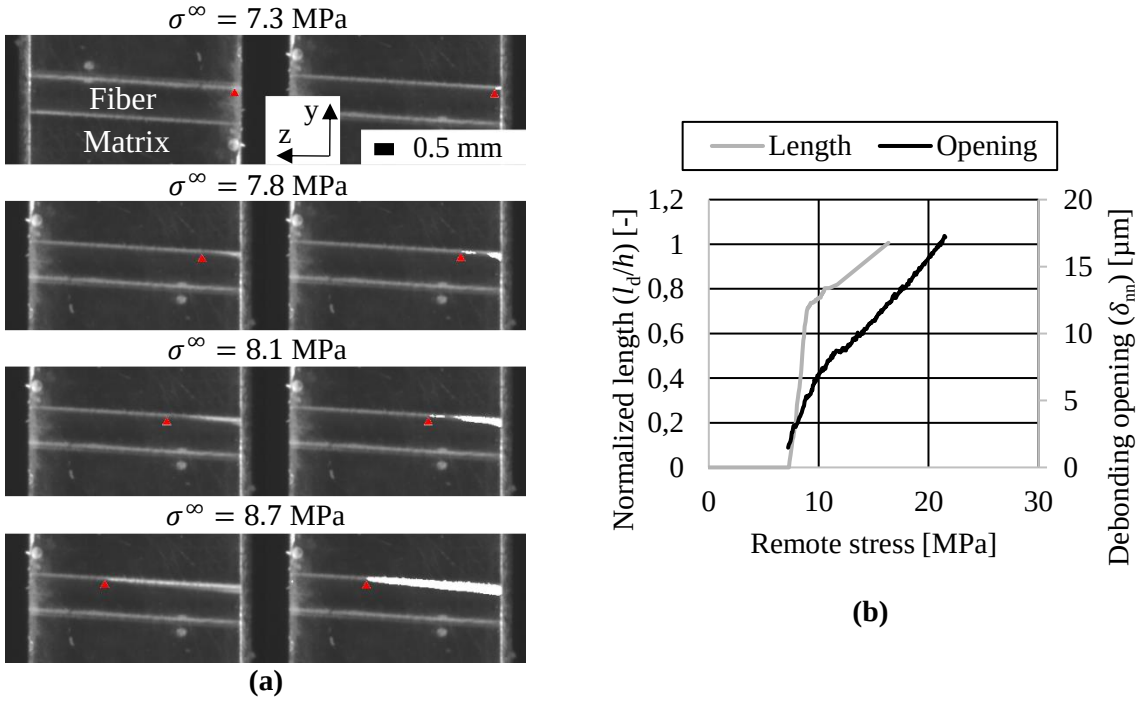

Figure 3. (a) Debonding propagation observed using the raw image, left column and using a threshold, right column. **(b)** Variation of both debonding length and opening as a function of the remote stress.

Figure 3b shows the variation in debonding opening and normalized length as a function of remote stress at the same debonding initiation site. The debonding length is normalized by the sample thickness *h*. Debonding initiation occurs at a remote stress of 7.2 MPa with both opening and length predictions being consistent. The maximum debonding opening at initiation are given in Table 2. Since debonding initiation occurs between two images, upper and lower bounds for debonding initiation opening can be determined.

Table 2. Debonding opening at initiation.

δ_{nn} [µm] lower bound	δ_{nn} [µm] upper bound
1.5 ± 1.0	1.7 ± 1.0

Difficulties in determining debonding angles are encountered experimentally. The pixel size obtained with the front camera varies between 10 and 12 µm, whereas the DIC provides debonding initiation opening with a sub-pixel size of 1 to 3 µm. Consequently, the resolution of the camera is not sufficient to capture the early stages of debonding at the free surface. Nevertheless, coupled experimental-numerical approach is established to retrieve the debonding angle and shape that best match the experimentally measured opening and debonding length. The approach consists of numerically comparing various debonding geometries approximated using a power-law of exponent 4. The appropriate geometry thus gives the debonding angle at the free surface and the shape of the debonding front. Identification can be performed at several debonding stages, providing debonding angles as a function of remote loading.

Debonding angles obtained from the coupled numerical-experimental approach are shown in Figure 4 by the white markers. The debonding angle can also be assessed using the side observation, using results from Figure 3a, shown by the solide line in Figure 4. The side observation method provides precise debonding angles for small angles only. For angles larger than 70 degrees, the difference in reflective index brought by the debonded zone is not sufficient to capture the actual debonding area. The mixed shear-compression loading causes the debonding area to be partially captured. Despite those differences, the proposed method offers an accurate description of the debonding angle for early stages of debonding.

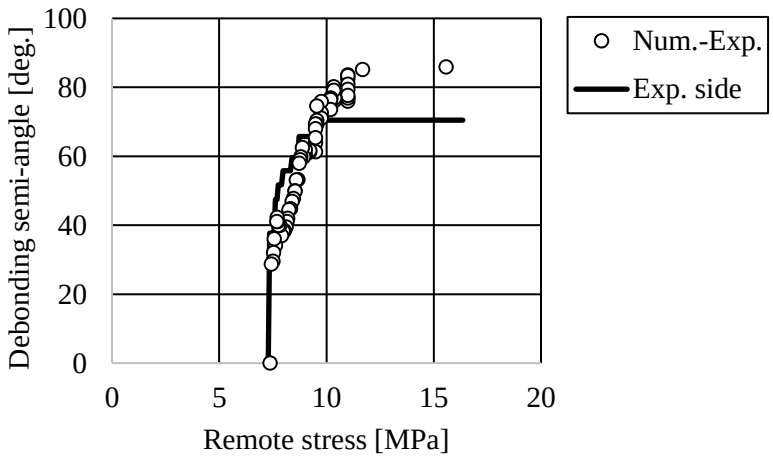

Figure 4. Variation of the debonding semi-angle as a function of the remote stress.

4. Conclusion

The proposed method enables the thorough description of the debonding process using different geometrical parameters. The extracted quantities provide key information such as the debonding initiation remote loading. Additionally, the debonding propagation can be monitored as a function of the remote stress. Experimental-numerical approach that couples experimental debonding opening and length to numerical results enables determining the debonding angle as a function of the remote loading. Debonding angle determined using the side observation is confirmed to be accurate except when the interface undergoes mixed shear-compression. Such experimental debonding observation can be used to calibrate an inverse identification approach that requires the debonding topology to be computed. Such inverse identification may enable the determination of the fiber-matrix interface fracture properties.

References

[1] Zhandarov, S., et E. Mäder. « Characterization of fiber/matrix interface strength: applicability of different tests, approaches and parameters ». Composites Science and Technology 65, nº 1 (2005): 149-60. https://doi.org/10.1016/j.compscitech.2004.07.003.

[2] Koyanagi, J., P. D. Shah, S. Kimura, S. K. Ha, et H. Kawada. « Mixed-mode interfacial debonding simulation in single-fiber composite under a transverse load ». Journal of Solid Mechanics and Materials Engineering 3, nº 5 (2009): 796-806. https://doi.org/10.1299/jmmp.3.796.

[3] Livingston, R., et B. Koohbor. « Characterizing fiber-matrix debond and fiber interaction mechanisms by full-field measurements ». Composites Part C: Open Access 7 (2022): 100229. https://doi.org/10.1016/j.jcomc.2022.100229.

[4] Girard, H., B. Koohbor, A. Doitrand, et R. Livingston. « Experimental characterization of in-plane debonding at fiber-matrix interface using single glass macro fiber samples ». Composites Part A: Applied Science and Manufacturing 171 (2023): 107573. https://doi.org/10.1016/j.compositesa.2023.107573.

[5] Ogihara, S., Y. Sakamoto, et J. Koyanagi. « Evaluation of Interfacial Tensile Strength in Glass Fiber/Epoxy Resin Interface using the Cruciform Specimen Method ». Journal of Solid Mechanics and Materials Engineering 3, no 9 (2009): 1071-80. https://doi.org/10.1299/jmmp.3.1071.

[6] Julien, Rethoré. « UFreckles ». Zenodo, 1 octobre 2018. https://doi.org/10.5281/ZENODO.1433775.